RSC Advances

PAPER

View Article Online
View Journal | View Issue

Cite this: *RSC Adv.*, 2026, **16**, 24080

Polymeric sorbent phase sorptive extraction for radiation metabolomics

Abdul Hoque,[a] Evan L. Pannkuk,[bcd] Jerome Lacombe,[ae] Sunil Bansal,[b] Jerry Angdisen,[b] Geraldine Vitry,[b] Abel Encarnacion Hernandez,[a] Nabhan M. Fakrudin,[a] Mathew Barrett,[a] James Helton,[a] Jian Gu,[a] Albert J. Fornace, Jr,[bcdf] Evagelia C. Laiakis[bcdf] and Frederic Zenhausern*[aeg]

Novel biodosimetry assays are needed for potential radiological incidents to rapidly assess radiation exposure and guide medical treatments. Mass spectrometry-based metabolomic analysis using a sorptive phase extraction is a rapid and efficient method for radiation-induced biomarkers in biofluids. Here, we developed a chemically functionalized polymeric Sorbent Phase Sorptive Extraction (SPSE) method. This method employs polymeric thin film sorbents with tailored organic functional groups, which directly bind radiation-responsive biomolecules and increase sample absorption capacity. This microporous membrane system enables rapid, high-sensitivity extraction of metabolites spanning a wide polarity range from urine, serum, and whole blood. We characterized the surface morphology, chemical functionality, and hydrophilicity of multiple sorbent-coated cellulose membranes, including plasma-functionalized nylon-6. Matrix interference was evaluated using untargeted metabolomics, and analytical performance was assessed using a targeted multiplex radiation biomarker panel. Urine, serum, and whole blood were collected from male and female C57BL/6 mice (9 weeks old) exposed to X-rays at 1 day (0, 2, 8, 13 Gy) and 7 days (0, 2, 8 Gy) post-irradiation. The membrane types preserve metabolite stability at room temperature for up to two weeks; however, nylon-6-based cellulose paper membranes exhibited the highest surface porosity, absorption capacity, and metabolite recovery. Classifier performance evaluated using receiver operating characteristic analysis demonstrated comparable sensitivity and specificity between SPSE and conventional dilute-and-shoot workflows. Collectively, these results support further development of polymeric sorbent coated paper and fabric-based substrates to increase throughput while eliminating cold-chain requirements. These environmentally conscious design features exemplify principles of green chemistry including lowering chemical waste and operational energy demand.

Received 30th January 2026
Accepted 30th April 2026

DOI: 10.1039/d6ra00832a

rsc.li/rsc-advances

Introduction

Large-scale exposure to ionizing radiation (IR) in the general population, whether from accidental or malicious sources, poses a potential threat and requires that response plans be established in such events.[1] One component of an adequate response will include sample transport and storage to testing facilities to determine if individuals have been exposed to IR and the level of acute radiation syndrome (ARS). These assays ideally provide measurements of metabolomic biomarkers for rapid dose assessment and triage in nuclear or radiation accidents that can guide medical treatments to thousands of exposed individuals.[2,3] However, during chaotic emergency events, in resource-limited environment, it would be beneficial to remove potential complications from sample transport and storage (*e.g.*, refrigerated equipment). These samples could then be stored for downstream high throughput analysis, such as liquid chromatography–mass spectrometry (LC–MS) based metabolomic analysis[4,5] that has been used for easily accessible biofluids,[6–8] including blood,[9–15] urine,[16–18] saliva.[19–22] An additional benefit would also reduce needed materials (*e.g.* solvents) and operational energy demand as critical infrastructure could be damaged.

[a]*Center for Applied NanoBiosience & Medicine, University of Arizona, Phoenix, Arizona 85004, USA. E-mail: fzenhaus@arizona.edu*

[b]*Department of Oncology, Lombardi Comprehensive Cancer Center, Georgetown University Medical Center, Washington, DC 20057, USA*

[c]*Department of Biochemistry and Molecular & Cellular Biology, Georgetown University Medical Center, Washington, DC 20057, USA*

[d]*Center for Metabolomic Studies, Georgetown University, Washington, DC 20057, USA*

[e]*Department of Basic Medical Sciences, College of Medicine Phoenix, University of Arizona, 85004, USA*

[f]*Department of Radiation Medicine, Georgetown University Medical Center, Washington, DC 20057, USA*

[g]*Honor Health Research Institute, Scottsdale, Arizona, 85260, USA*

Collecting and preparing biological samples for the assessment of IR-induced biomarkers from such a large population would ideally incorporate a process that is fast, cost effective, and robust compared to classical sample preparation techniques.[23] For this purpose, a pragmatic and easily accessible platform is required that ensure simplicity, scalability, and make it suitable for point-of-care (POC) applications, where only a minimal blood volume, such as a finger-prick sample, is needed for rapid biomarker extraction and stabilization. Such capability could enable high-throughput screening and triage of large populations following a radiological incident, thereby accelerating first-responder decision-making and improving the timeliness of medical countermeasures.[24] The standard "dilute-and-shoot" sample preparation entails five primary pretreatment steps: solvent addition, mixing, centrifugation, protein precipitation, and aliquot transfer.[25] Furthermore, blood is typically separated into either serum or plasma before sample preparation.[26] These sample processing steps require use of large volume of hazardous organic solvents and are typically performed in refrigerated equipment which inherently introduces analytical variation, sample loss, possible human error, and time delays during this process.

Green chemistry-based sample preparation for biomolecules extraction considers minimizing hazardous solvent use and energy consumption, require minimal sample volume, and maximize sample throughput.[27–29] The practical applicability, simplicity and economic feasibility also the important parameters for the development of green analytical sample preparation methods.[30–32] Our approach mainly relies on the elimination of the cold chain logistics for sample storage, miniaturized extraction platforms, and energy efficient methods for high-throughput large-scale sample analysis. In addition, in the context of a mass-casualty radiological scenario, the usefulness of a metabolomic study is constrained by the sample timing, cold-chain logistics, standardization, and biological confounders *etc.*[33] Complications that can arise from cold chain management have been recently documented from the delivery of SARS-CoV-2 vaccinations, the need and maintenance of laboratory freezers for storage and transport during an emergency situation posed a great challenge.[34] Radiation responsive metabolites could be transient and require faster sampling. Therefore, the ideal approach would be to develop a high-throughput sample collection strategy, preferring dried blood spots or other biofluids in a membrane that can stabilize the markers during transportation. *In situ* sample preparation can save energy and time for such events that require a large number of sample collection in an emergency response.[35] Developing an advanced sample preparation technique for metabolomic analysis that can eliminate cold-chain logistics, reduce hazardous solvent use, and facilitate large scale *in situ* sample collection is a need for a radiological emergency or similar mass-casualty events.[36]

Fabric Phase Sorptive Extraction (FPSE)[37] is an established sample preparation technique for the sorptive extraction of different compounds from various sample types such as, environmental,[38–40] pharmaceuticals,[41,42] biological,[43,44] textile materials,[45,46] food[47,48] and non-invasive exhaled breath aerosol sample *etc.*[49] A wide range of compounds, such as drug molecules,[50–52] polycyclic aromatic hydrocarbons (PAHs),[53,54] and toxic heavy metals,[55,56] have been successfully extracted from different sample types mentioned above using this technique. However, small molecule biomarkers extraction from whole blood or serum using FPSE sample preparation method is still limited.[44,57,58] The selectivity and extraction efficiency depends on the surface chemistry or sample absorption properties of FPSE membrane. The polymeric sorbent improves surface porosity, chemical functionality and hydrophilic properties of the membrane that help to better permeate the sample matrix through the FPSE membrane and increase the extraction efficiency of target metabolites.[58] Since polymeric sorbent improves the thermal, mechanical, and even chemical stability of the FPSE membrane, it is an excellent medium for long time sample storage without any preservatives. Therefore, the FPSE method offers many advantages in the sample preparation that include: (i) simpler workflow, (ii) refrigeration, (iii) small volume of elution solvent required,[59] (iv) use of any solvent for back extraction, (v) eliminating/minimizing sample pretreatment steps, (vi) minimal sample volume required,[60] and (vii) maximize biomolecular extraction efficiency from whole blood.[61] We aim to utilize the FPSE method as a field deployable format to capture and stabilize analytes at the point of collection at ambient temperature to establish a fast, scalable, and low-cost sample processing platform for metabolomic analysis.

In this study, we expanded some features and the utility of FPSE to increase sample absorption and aid in the user-interface and efficiency of biofluid preparation for metabolomics based biodosimetry. We used polymeric sorbent phase sorptive extraction (SPSE) technique that uses thin film of sorbent on the fabric/paper substrates using variable concentrations of polymeric coatings to develop a field-deployable efficient extraction platform. This SPSE membrane can stabilize metabolites, maximize extraction efficiency, and eliminate drawbacks associated with sample preparation for rapid biomarker assessment. In the unexpected nuclear or radiological events, such as nuclear accidents or act of terrorism,[62] there is an urgent need to rapidly and accurately collect the samples from a large number of individuals who are exposed to radiation. Therefore, it is important to categorize those exposed individuals into different dose and exposure types for the treatment plans. We previously found cellulose based membranes provided increased temporal stabilization of a blood-based radiation biomarker panel.[44] The present study reports improvements with the development of novel cellulose membranes with more hydrophobic polymeric sorbent coatings to test in our standardized biodosimetry pipeline with additional types of biofluids (urine, whole blood, and serum). We characterized surface morphology, functionality, and hydrophilicity of novel sorbents. The utility of these new materials in MS-based biodosimetry analysis was assessed by both untargeted and targeted metabolomics using the murine model. Lastly, we developed a high-throughput 12-well plates sample preparation device that was developed using SPSE membrane considering a radiological emergency or such mass-casualty scenario to collect large number of blood samples in the point

of collection. Overall, this technology would contribute to address some post-logistical gaps of a radiological emergency response, including reducing the need for specialized equipment in sample shipping and storage.

Materials and methods

Chemicals and materials

Nylon-6 polymer (pellet) and formic acid (ACS reagent grade ≥96%) were purchased from Sigma-Aldrich (Saint louis, Missouri, USA). The cellulose fabric substrate (100% cotton, sew essentials unbleached) was purchased from JoAnn (Phoenix, AZ, USA) and cellulose paper substrate (Whatman™ 3 MM Chromatography Paper) was purchased from Fisher Scientific (Thermo Fisher Scientific™ Inc., Waltham, MA). Solvents for metabolomics sample preparation and LC–MS analysis were purchased from Optima™ grade (Thermo Fisher Scientific™ Inc., Waltham, MA, USA). Chemical standards included: chlorpropamide, L-carnitine, taurine, citrulline, hypoxanthine, Nε,Nε,Nε-trimethyllysine hydrochloride (TML), azelaic acid (Sigma-Aldrich, St. Louis, MO, USA); C18 sphingomyelin (d18:0/18:0), sphinganine d7 (d18:0) (Cayman Chemical Company, Ann Arbor, MI, USA); L-carnitine d3 HCl, taurine d4, citrulline d7, hypoxanthine-d4, Nε,Nε,Nε-trimethyl-d9-lysine hydrochloride (TML-d9), L-citrulline d7, and acetyl-d3-L-carnitine (CDN isotopes, Pointe-Claire, QC, Canada). NIST plasma Standard Reference Material (SRM) 1950 (plasma) and 3667 (urine) were used as quality control samples (Gaithersburg, MD, USA).

Sorbent preparation and membrane development

Different concentrations of nylon-6 sorbent solution were prepared using formic acid as a solvent. To prepare 0.5%, 1.0%, and 1.5% nylon-6 solution, 0.5 g, 1.0 g, or 1.5 g of nylon-6 pellet were added into 100 ml of reagent grade formic acid (≥95%), respectively. The solution was continuously stirring with 500 rpm at 50 °C for 8 h to dissolve nylon-6 pellet completely and prepare a homogenous solution. Two more polymeric sorbents such as methacrylated chitosan (MC) and 3-aminopropyl-triethoxysilane (APTES) grafted chitosan (CA) were prepared along with nylon-6 for comparative study to identify the best sorbent materials for the targeted biomarker extraction. MC was synthesized based on previous work.[63] A 1.5 g of chitosan were added into 100 mL of 4% v/v acetic acid and the solution was stirred at 50 °C overnight to dissolve completely. Nine ml of methacrylic anhydride were added dropwise into chitosan solution and the mixture was stirred for another 12 hours at 50 °C to complete the synthesis. APTES functionalized chitosan was prepared following a similar protocol with a mixture of 2 g of chitosan and 1 g of APTES into 100 mL of 4% v/v acetic acid and then the mixture was stirred at 50 °C for 12 hours to complete the process.

Prior to applying sorbent materials on the commercial cellulose fabric substrate, a pretreatment/mercerization process was performed to remove all the residual chemicals such as additives, dye, and fillers from the substrate. A piece of fabric (3 × 3 inches) substrate was soaked into deionized water followed by treatment with a 1 M NaOH solution for 1 h with sonication. The fabric was then washed with deionized (DI) water multiple

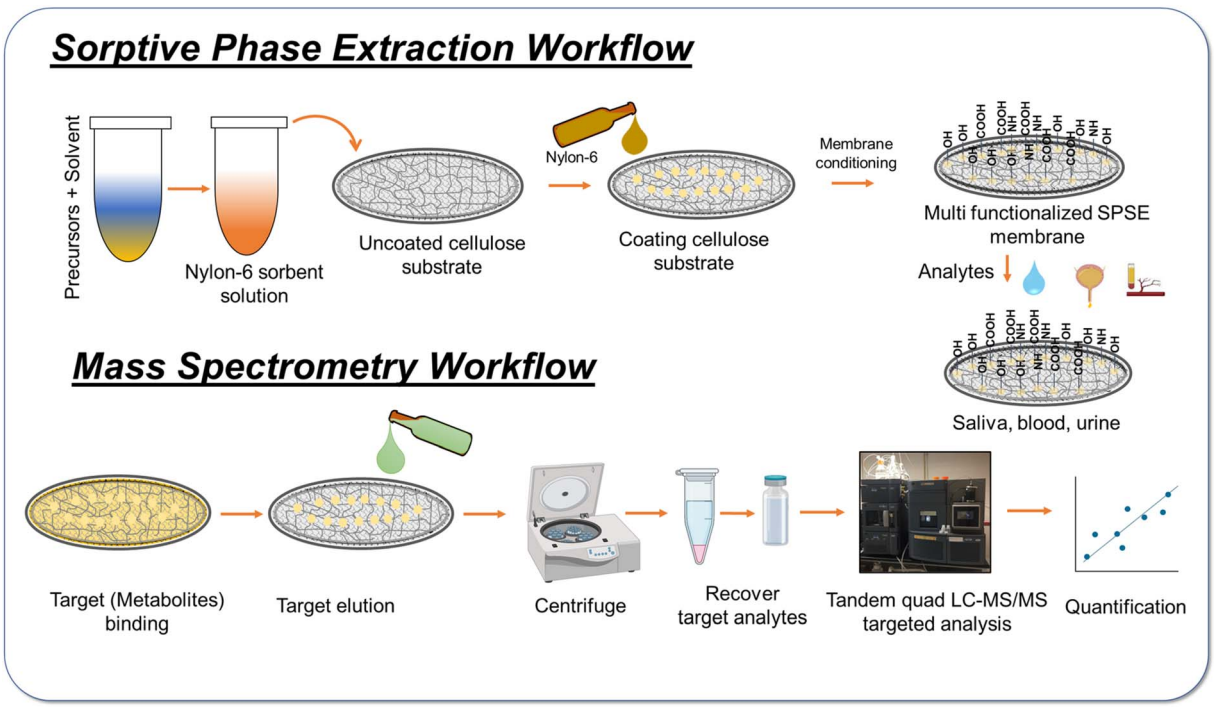

Fig. 1 Schematic illustration of sorbent phase sorptive extraction process and LC–MS/MS workflow for radiation targeted metabolomic analysis. The routes of sorbent preparation, coating cellulose substrate, plasma activation for SPSE membrane development, and biofluid absorption, target elution and quantification using LC–MS/MS analysis.

times followed by soaking again into 0.1 M HCl solution for 1 h under sonication. The acid-treated fabric was washed with copious amount of DI water multiple times and dried at 70 °C in an argon environment. The cleaned cellulose fabric substrate was then dipped coated with different concentrations of nylon-6 (0.5%, 1.0%, 1.5%) solution with 3 dips (30 s dip and 30 minutes dry after each dip at room temperature). The membrane was then annealed at 70 °C in an argon medium overnight to evaporate solvent completely. To improve the hydrophilic interactions of nylon-6 coated SPSE membrane, we applied 60 s of oxygen plasma on the surface using Harrick PlasmaFlo. The SPSE membrane was placed inside the plasma chamber and cleaned the chamber with ultrahigh purity nitrogen gas, and purge oxygen gas before final pump down. The membrane was treated with oxygen plasma with low pressure (300 mtorr) at 25 W in high frequency (10 MHz) with medium flow rate. The cellulose paper membrane was prepared using a similar protocol without pretreatment steps.

MC and APTES grafted chitosan sorbents were applied in the same dip coating process with 1, 5, and 10 dips and annealed at 70 °C for 12 hours in an argon environment. All the membranes were then laser cut into 10 mm × 10 mm circular disc using versa laser for downstream biological sample processing. Fig. 1 shows the schematic illustration of sorptive phase extraction that indicates multi-steps process of SPSE membrane development and LC–MS/MS workflow for biomarker analysis. SPSE is a deployable technique which can be used for high throughput sample preparation in the radiological emergency with minimal sample volume (~5 μL) with rapid, robust, and high trueness. The goal of these studies is to minimize logistical issues associated with the need for refrigerated equipment during sample delivery and storage, as was encountered during distribution of COVID-19 vaccinations.[34]

Physical and chemical characterization

The detailed characterization of SPSE membranes were performed by various microscopic and spectroscopic techniques. The surface chemical functionalization of coated and uncoated membranes was analyzed using Fourier Transform Infrared Spectroscopy (FTIR) (Nicolet Is50, Thermo Fisher Scientific, Madison, WI, USA) and X-ray Photoelectron Spectroscopy (XPS) (Shimadzu, Kyoto, Japan). The XPS analysis was conducted by Kratos Axis Ultra 165 photoelectron spectrometers to investigate the oxygen-containing functional groups using Al Kα monochromatic X-ray source before and after plasma treatment. XPS data acquisition and analysis were performed by Kratos Vision2 Processing software, and all core level peaks were calibrated based on C 1s peak at 284.8 eV for charging effect correction. The surface morphology of both fabric and paper membranes were characterized by Zeiss Auriga Scanning Electron Microscopy (SEM) (Jena, Germany) to evaluate the sol–gel materials and surface porosity before and after coating. The surface area, pore volume and pore size of the coated and uncoated membranes were characterized by Micromeritics TriStar II Plus (Georgia, USA) at 77 K using N_2 gas. The wettability of the SPSE membranes was studied by water contact angle measurements using the ramé-hart instrument (New Jersey, USA).

Animal model, radiation exposure, and biofluid collection

Male ($n = 5$ per group) and female ($n = 5$ per group) 8–10 weeks old C57BL/6 mice (C57BL/6NCrl strain code #027) were ordered from Charles River Laboratories (Frederick, MD). Animals were housed at Georgetown University (12 h light/12 h dark cycle conditions) with water and food (PicoLab Rodent Diet 20 # 5053) provided *ad libitum* according to Georgetown University Institutional Animal Care and Use Committee (GUACUC) protocols (IACUC protocol # 2016-1152). Mice were irradiated after placing them in a 12-slot acrylic mouse pie cage (MPC-1, Braintree Scientific, Braintree, MA) that was on a turntable. Mice were exposed to a total body irradiation (TBI) X-ray dose (14.7 mGy s; XRAD 320, Precision X-ray Inc, Branford, CT; filter, filter of 0.75 mm tin/0.25 mm copper/1.5 mm aluminum with a half value layer of ~3 mm Cu at 50 cm from source) of 0, 2, 8, or 13 Gy. Dosimetry was performed with a Radcal 10 × 6–6 in Beam Chamber (Monrovia, CA). Spot urine samples were collected at selected time points post-irradiation [1 day (0, 2, 8, 13 Gy) and 7 days (0, 2, 8 Gy)]. Blood for metabolomics was collected by cardiac puncture at the same endpoints, with whole blood separated immediately after collected into a BD Microtainer blood collection tube with K2EDTA (BD Cat # 365974) and into a BD microtainer serum separator tube (BD Cat # 365976) and centrifuged for 10 min (2000×*g*, 4 °C). All biofluids were flash frozen in liquid nitrogen and stored at −80 °C until further use.

Membrane preparation and LC–MS

Membranes were initially washed in 50% acetonitrile (ACN) for 5 seconds and dried under vacuum for 24 h. Biofluids [whole blood or serum (5 μL) or urine (10 μL)] were added to dried SPSE membranes and left under vacuum for the duration of each particular time point (1 day unless specified otherwise). Membranes were then transferred to a 1.5 ml Eppendorf tube with 100 μL solvent (66% ACN whole blood and serum; 50% ACN urine). Samples were shaken 10 min at max speed at 15 °C on an Eppendorf Thermomixer R. Membranes were removed and the supernatant was centrifuged for 10 min (10 000×*g*, 4 °C). A 40 μL aliquot of the supernatant was recovered and diluted with 40 μL solvent (66% ACN whole blood and serum; 50% ACN urine) containing internal standards [final concentration (1 μM): carnitine (d3), TML (d9), sphinganine (d7); (2 μM): chlorpropamide, taurine (d4); (3 μM): hypoxanthine (d4), creatinine (d3), citrulline (d7), malic acid (d3), citric acid (d4)] and injected for LC–MS analysis. For comparison to biological samples, we deproteinated biofluids by mixing with cold solvent [whole blood or serum (5 μL, 66% ACN) or urine (10 μL, 50% ACN)], vortexed the samples, centrifuged for 10 min (10 000×*g*, 4 °C), and diluted a 40 μL aliquot of the supernatant with 40 μL solvent and internal standards as above. Optimization of extraction solvent and time was performed by applying a 10 μL standard solution [carnitine, taurine, TXB2, Sphingomyelin (d18:0/18:0), GlcCer (d18:124:1), Ceramide (d18:1/18:1), final

Table 1 Multiple reaction monitoring transitions, parameters, and R^2 of standard curve for quantification

Metabolite	Mode	Parent ion (m/z)	Daughter ion (m/z)	Dwell time (sec)	Cone (eV)	Collision (eV)	R^2	LOD (nM)	LOQ (nM)	RT (min)	Biofluid
Carnitine	ESI^+	162.3	85.0	0.003	34	20	0.99	0.2	0.6	0.40	Urine/ whole blood/ serum
Carnitine (d3)	ESI^+	165.0	85.0	0.025	2	16	—	—	—	0.39	—
Taurine	ESI^-	126.0	44.0	0.003	24	14	0.98	12.2	48.8	0.37	Urine/ whole blood/ serum
Taurine (d4)	ESI^-	130.0	48.2	0.025	70	14	—	—	—	0.36	—
Citrulline	ESI^+	176.0	69.9	0.003	16	20	0.82	19.5	39.1	0.58	Whole blood/ serum
Citrulline (d7)	ESI^+	183.1	77.0	0.003	28	20	—	—	—	0.58	—
SM	ESI^+	731.6	184.2	0.003	52	27	0.83	31.3	62.5	5.34	Whole blood/ serum
Sphinganine (d7)	ESI^+	309.3	273.4	0.003	80	16	—	—	—	1.53	—
Chlorpropamide	ESI^-	275.1	126.1	0.025	52	30	—	—	—	7.68	Urine
Chlorpropamide	ESI^+	277.1	111.1	0.025	32	36	—	—	—	0.77	Whole blood/ serum
Creatinine	ESI^+	113.8	86.1	0.003	46	14	0.94	9.8	39.1	0.46	Urine
Creatinine (d3)	ESI^+	116.9	89.1	0.003	2	10	—	—	—	0.47	—
TML	ESI^+	183.1	84.0	0.003	40	20	0.92	0.6	2.4	0.42	Urine
TML (d9)	ESI^+	198.1	130.1	0.025	4	14	—	—	—	0.42	—
Hypoxanthine	ESI^+	137.1	109.9	0.003	44	20	0.96	2.4	39.1	0.46	Urine
Hypoxanthine (d4)	ESI^+	141.2	113.0	0.003	25	18	—	—	—	0.47	—

concentration 1 μM] to 0% and 0.5% nylon-6 membranes, incubating them for 24 h at room temperature under vacuum, extracting with 50% ACN, 50% methanol, 40% ACN/40% methanol for 5, 10, and 30 min, and then comparing to a standard solution prepared by the above standard protocol.

Untargeted metabolomic profiling was used to test matrix interference and separation of biofluids from irradiated animals compared to sham-irradiated mice. SPSE processed samples were injected (2 μl) and analyzed by Waters Acquity Ultra Performance (UP) LC coupled to a Xevo® G2S quadrupole time-of-flight (QTOF) MS (Waters, Milford, MA, USA). The UPLC was equipped with an Acquity BEH C18 1.7 μm, 2.1 × 50 mm column kept at 40 °C for urine and 60 °C for whole blood and serum. Data were collected in both negative and positive electrospray ionization (ESI) data independent acquisition modes and were run with leucine enkephalin, 556.2771 $[M + H]^+$ or 554.2615 $[M - H^-]$, used as LockSpray™. Mobile phase separation for urine was achieved using water/0.1% formic acid (FA) and ACN/FA. The flow rate was 0.5 ml min^{-1} with a gradient of 4.5 min 5% ACN/FA, 4.0 min 20% ACN/FA, 5.1 min 95% ACN/FA, and 1.9 min 5% ACN/FA. Mobile phase separation for whole blood and serum was achieved using water/FA, ACN/FA, isopropanol (IPA)/FA. The flow rate was 0.5 ml min^{-1} with a gradient of 4.5 min 2% ACN/FA 0% IPA/FA, 4.0 min 60% ACN/FA 0% IPA/FA, 1.5 min 98% ACN/FA 0% IPA/FA, 2.0 min 11.8% ACN/FA 88.2% IPA/FA, 0.5 min 50% ACN/FA 0% IPA/FA, and 1.0 min 2% ACN/FA 0% IPA/FA.

For targeted analysis, SPSE processed samples were injected (5 μl) and analyzed with a Waters Acquity UPLC coupled to a Xevo® tandem quadrupole (TQ-S) MS operating in multiple reaction monitoring (MRM) mode (Waters, Milford, MA, USA). The UPLC was equipped with an Acquity BEH C18 1.7 μm, 2.1 × 50 mm column kept at 40 °C for urine and an Acquity CSH C18 1.7 μm, 2.1 × 50 mm column 60 °C for whole blood and serum kept at 60 °C. MRM transitions were developed using the "IntelliStart" feature in MassLynx (Table 1) using nominal mass with the MS/MS collision energies between 10–20 eV. Mobile phase separation for urine was achieved using water/1 mM ammonium formate and ACN/FA. The flow rate was 0.5 ml min^{-1} with a gradient of 4.5 min 5% ACN/FA, 4.0 min 20% ACN/FA, 1.1 min 95% ACN/FA, and 1.1 min 5% ACN/FA. Mobile phase separation for whole blood and serum was achieved using water/ACN (1 : 1) FA and 1 mM ammonium formate, and IPA/ACN (9 : 1) FA and 1 mM ammonium formate. The flow rate was 0.45 ml min^{-1} with a gradient of 5.0 min 40% IPA/ACN (9 : 1) FA and 1 mM ammonium formate, 1.0 min 100% IPA/ACN (9 : 1) FA and 1 mM ammonium formate.

To test for recovery and stability of standards applied to membranes, we applied standards at a final working concentration of 5 μM and left at room temperature under vacuum. Samples were collected at 1 day for recovery and at 1, 5, and 14 days for stability. For untargeted metabolomics, we inspected the raw data files in MassLynx v.4.1 (Waters Corporation, Milford, MA) before data pre-processing with progenesis QI (Nonlinear Dynamics, Newcastle, UK), which was used for peak alignment using software chosen QC chromatogram, peak picking, and normalization (normalize to all compounds functions). The data matrix was imported into the online software MetaboAnalyst 5.0 (log transformed and pareto scaled) to generate PCA plots.[64] For targeted metabolomics, data files were processed in the software TargetLynx. We prepared a standard solution of all metabolites using a 4-fold dilution representing the dynamic range of 0.0005–10 μM to construct 10-point calibration curves. Calibration curves were fitted using the nonlinear regression function without the Y intercept constrained to zero. Values were plotted in GraphPad Prism 9.2.0 and checked for outliers (ROUT $Q = 1\%$) (GraphPad Software, La Jolla, CA, USA). Receiver operating characteristic (ROC) curves were generated in MetaboAnalyst 6.0 to calculate the area under the curve (AUC) as a measure of the sensitivity and specificity.[65]

Results & discussion

SPSE membrane development

A SPSE technique was employed to prepare different biofluid samples, such as whole blood, urine, and serum, to assess signal suppression for multiplex assays and evaluate the stability and recovery of different biomarkers from irradiated mice. SPSE is a preparative analytical technique that simplifies the sample preparation for efficient extraction of biomarkers, maintains metabolite stability and accelerates the sample processing using the minimal sample volume possible. Here, we have developed different types of cellulose paper and fabric membranes using three different sorbents including nylon-6, MC, and APTES-grafted chitosan, for initial testing. To investigate the physiochemical properties of the membranes, we characterized the surface morphology, organic functionality, and hydrophilicity using different microscopic and spectroscopic techniques. The surface chemical functionality of cellulose fabric and paper membranes was characterized by FTIR spectroscopy. The comparative FTIR spectra of fabric and paper membranes are presented in Fig. 2. The uncoated cellulose fabric (Fig. 2A, black line) and paper (Fig. 2B, black line) substrates show broad peak at 3298 cm^{-1} (–O–H stretching), –C–H stretching vibration at 2914 cm^{-1}, and –C–O–C pyranose ring skeletal vibration at 1061 cm^{-1}. Nylon-6 coating on cellulose substrates (both fabric and paper) added carbonyl (C═O) functional group at 1636 cm^{-1} (stretching bend) and C–N stretching at 1535 cm^{-1}, indicating the successful coating on cellulose substrate. Other N–H stretching bands from amino groups might be overlapped on O–H stretching at 3298 cm^{-1}. The FTIR peak intensity (Fig. 2A and B) related to the C═O and C–N stretching band increased as the concentration of nylon-6 sorbent increased in both cellulose fabric and paper substrate. Additionally, the paper membrane showed a greater adsorption of nylon-6 on the surface compared to the fabric substrate because of the greater peak heights (Fig. 2B) observed for similar stretching bands (C═O, C–N) at 1636 cm^{-1} and 1535 cm^{-1}, respectively. The diverse chemical functionality presents in nylon-6 coated cellulose membranes are key components that can chemically bind metabolites from different biofluids. The membrane that contains different oxygen-containing groups such as –OH, –COOH, C═O, primary

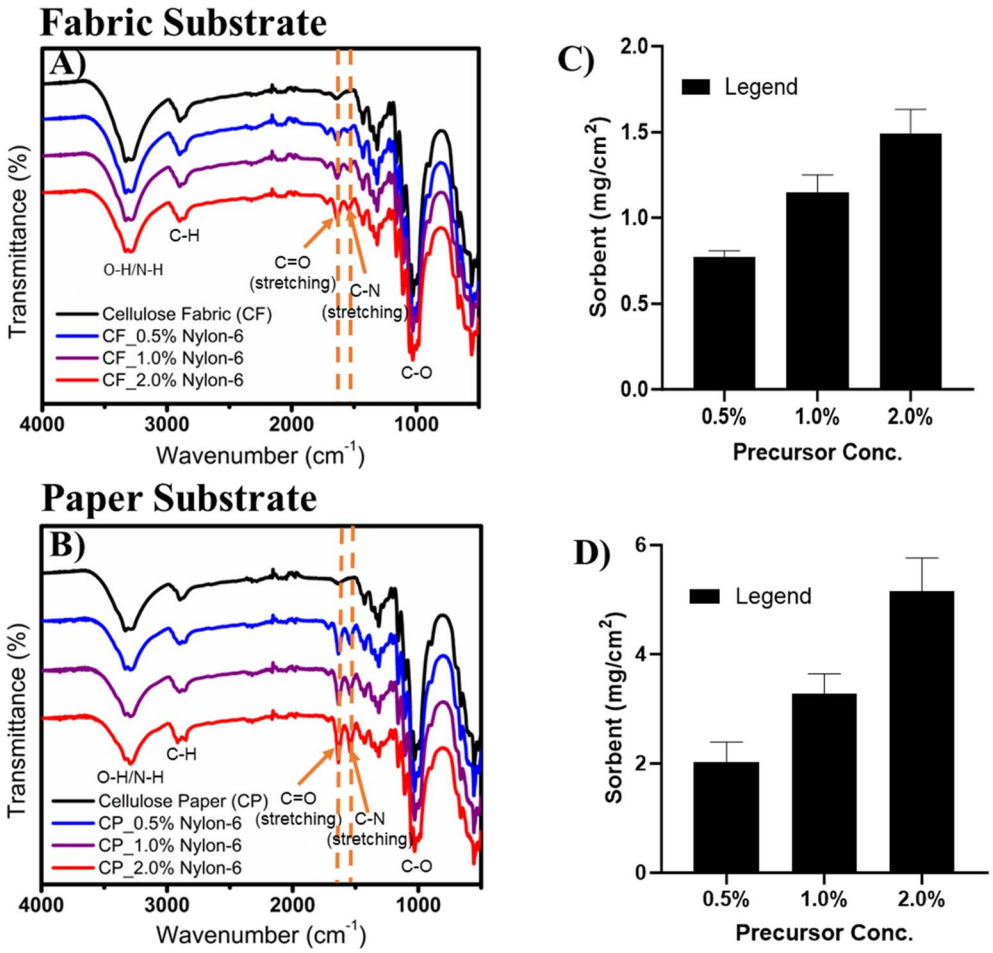

Fig. 2 FTIR spectra and bar graphs of nylon-6 sorbent coated SPSE membranes. (A) FTIR spectra of uncoated and sorbent coated cellulose fabric membranes and (B) cellulose paper membranes with different concentrations of nylon-6 solutions. (C) Bar charts indicating the amount of nylon-6 sorbent loaded onto cellulose fabric substrate and (D) cellulose paper substrate with respect to the concentration of nylon-6 solution.

and secondary amines (–N–H, $–NH_2$), and long hydrocarbon chain ($–CH_2–$) can interact with both polar and non-polar biomarkers.

MC and APTES grafted chitosan membranes were characterized by FTIR, which are presented in the SI section (Fig. S1) to confirm the successful coating on the cellulose substrate. FTIR spectra of MC-coated membrane (Fig. S1A) showed characteristic carbonyl (C═O) stretching band at ~1713 cm^{-1} and C–N stretching at 1560 cm^{-1}, indicating successful coating on the cellulose surface. The hydroxyl peak in the range of 3200 to 3450 cm^{-1} for MC-coated membrane showed deformation because of N–H stretching from amino group overlapping in the same region also confirm the MC sorbent present in the surface. APTES functionalized chitosan coating on the cellulose substrate was identified in Fig. S1B that indicated the C–N stretching peak at 1560 cm^{-1}. The sorbent materials coated on both cellulose fabric and paper substrates using dip coating technique were measured with respect to concentrations of the polymeric solution. The bar chart presented in Fig. 2C (Fabric) and 2D (Paper) indicates the amount of nylon-6 sorbent loaded into the cellulose substrate. To develop a nanoscale coating on the surfaces of both fabric and paper substrates, we used three different concentrations (0.5, 1.0, or 2.0%) of nylon-6 sorbent solution. It was observed that increasing the concentration of nylon-6 increased the amount of sorbent material (Fig. 2C and D) after coating on the surface of both fabric and paper substrates. The maximum amount of sorbent (1.5 mg cm^{-2}) was loaded into cellulose fabric substrates using 2.0% of nylon-6 solution. However, the cellulose paper substrate showed better performance in capturing more nylon-6 sorbent on the surface compared to cellulose fabric substrate. The maximum amount of 5.16 mg cm^{-2} sorbent was loaded into cellulose paper substrate using 2.0% nylon-6 solution, whereas fabric substrate absorbed 1.5 mg using a similar concentration.

Both cellulose fabric and paper substrates are made up of cellulose microfibrils that create interstices, voids, and nanoscale pores on the surface. Dip coating polymeric sorbent solution on the surface allows the polymeric materials to permeate through the wall of cellulose microfibrils, and upon annealing, nanoscale pores can form on the coated materials. The morphological characterization was conducted using SEM for both bare cellulose substrates and SPSE membranes to

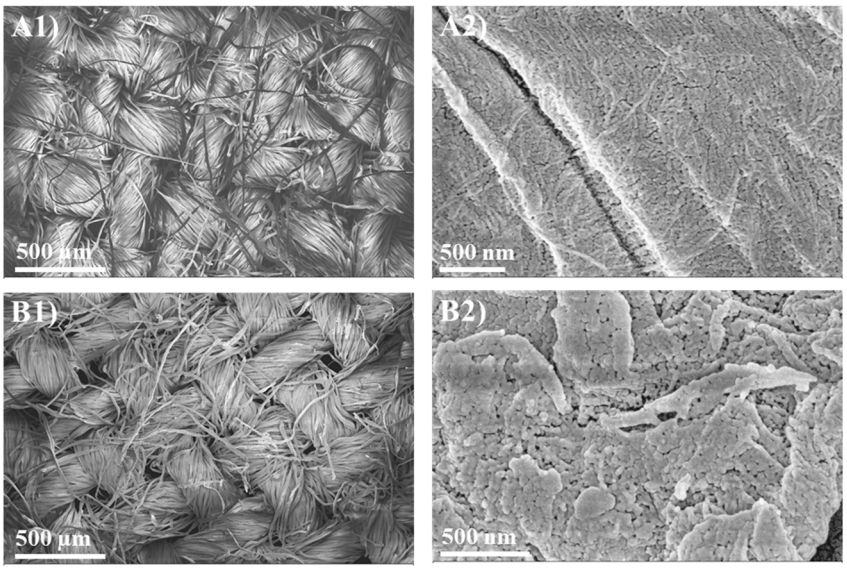

Fig. 3 SEM images of uncoated cellulose fabric substrate and nylon-6 coated cellulose fabric membrane using scanning electron microscopy (SEM). (A1 & A2) Low magnification and high magnification SEM images of uncoated cellulose fabric substrate, (B1 & B2) SEM images of nylon-6 coated cellulose fabric membrane.

confirm the presence of coating materials and the surface morphology. The SEM images of uncoated cellulose fabric substrate (Fig. 3, A1 and A2) and 0.5% nylon-6 coated cellulose fabric membrane (Fig. 3, B1 and B2) revealed differences in their morphology. The high magnification SEM images (Fig. 3, A2 and B2) clearly indicate the presence of coating materials on the cellulose fabric membrane and heterogeneous nanoscale porosity on the surface. The surface nanopores can increase the sample absorption properties, which increase the physicochemical interaction of metabolites to the membrane surface that maximize biomarker extraction. The similar surface characterization of cellulose paper membrane presented in SI section (Fig. S2) before and after coating. Fig. S2A2 indicates the cellulose paper membrane that is coated with 0.5% nylon-6 polymer, which shows clear distinctions from the uncoated cellulose paper substrate (Fig. S2A1). Surface analysis of both paper and fabric membranes were performed by Brunauer–Emmett–Teller (BET) N_2 adsorption–desorption studies.

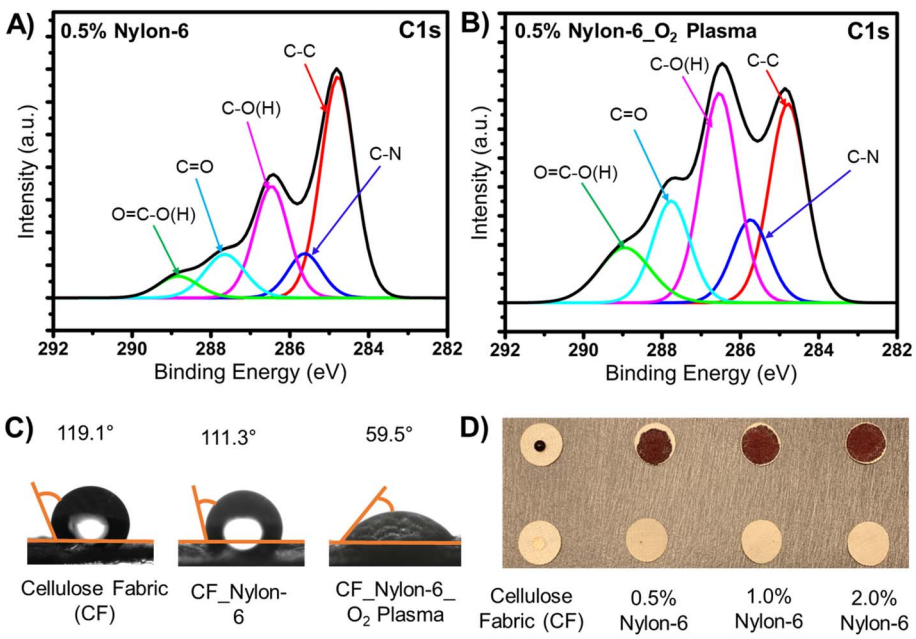

Fig. 4 X-ray photoelectron spectroscopy (XPS) analysis, contact angle measurement, and blood absorption capacity of nylon-6 coated SPSE membranes before and after plasma activation. (A) XPS core level C 1s spectra of untreated nylon-6 coated membrane and (B) 60 s oxygen plasma-treated membrane (C) contact angle measurement of uncoated cellulose substrate and 0.5% nylon-6 coated SPSE membrane, and (D) real sample (whole blood and serum) absorption capacity study for both untreated and plasma-treated membranes.

Table 2 Extraction efficiency for representative polar and non-polar metabolites from 0 and 0.5% nylon-6 sorbents (paper membrane) for different solvents and times. The $n = 3$ per group with values expressed as percentage compared to a standard mixture prepared using a typical 50% acetonitrile sample preparation

	0% Nylon			0.5% Nylon		
	50% ACN	50% MeOH	40% ACN/40% MeOH	50% ACN	50% MeOH	40% ACN/40% MeOH
Carnitine	86 ± 4	84 ± 0	49 ± 2	73 ± 3	70 ± 5	43 ± 1
Taurine	71 ± 9	71 ± 2	68 ± 10	63 ± 2	65 ± 7	62 ± 4
TXB2	109 ± 11	116 ± 14	105 ± 15	122 ± 20	98 ± 16	102 ± 14
Sphingomyelin (d18:0/18:0)	21 ± 3	0 ± 0	203 ± 24	14 ± 1	0 ± 0	178 ± 28
GlcCer (d18:1/24:1)	18 ± 3	1 ± 0	443 ± 20	13 ± 4	1 ± 0	335 ± 42
Ceramide (d18:1/18:1)	11 ± 5	2 ± 1	180 ± 18	7 ± 3	2 ± 0	136 ± 33
	5 min	10 min	30 min	5 min	10 min	30 min
Carnitine	102 ± 1	95 ± 6	80 ± 2	67 ± 6	68 ± 1	68 ± 2
Taurine	82 ± 3	66 ± 15	59 ± 3	67 ± 2	67 ± 5	62 ± 1
TXB2	128 ± 4	112 ± 10	88 ± 21	103 ± 6	105 ± 4	98 ± 9
Sphingomyelin (d18:0/18:0)	87 ± 1	81 ± 8	73 ± 14	94 ± 6	78 ± 10	94 ± 6
GlcCer (d18:1/24:1)	47 ± 4	61 ± 9	59 ± 19	47 ± 4	46 ± 8	64 ± 7
Ceramide (d18:1/18:1)	64 ± 2	64 ± 11	68 ± 11	62 ± 6	64 ± 5	107 ± 4

Adsorption–desorption isotherm and pore volume *vs.* pore diameter graphs of paper (Fig. S2B1 and S2B2) and fabric membranes (S2C1, S2C2) are presented in Fig. S2 in the SI section. It is observed that the uncoated cellulose paper substrate has surface area of 1.034 $m^2 g^{-1}$, pore volume is 0.006 $cm^3 g^{-1}$ and average pore diameter 26. 05 nm, whereas nylon-6 coated paper membrane showed surface area 1.304 $m^2 g^{-1}$, pore volume 0.009 $cm^3 g^{-1}$, and average pore diameter 27.6 nm, respectively. Therefore, 20.7% of surface area and 33.3% pore volume increased after nylon-6 polymeric coating of SPSE paper membrane. On the other hand, cellulose fabric substrate showed slight decrease in surface area (2.54%) and pore volume (16.63%) after sorbent coating which might be the predominance of macropores present on the surface.

We previously demonstrated that biomarker release was related to its physicochemical adhesion, with higher efficiency observed for hydrophilic substrates (cellulose) compared to hydrophobic substrates (fiberglass).[44] Therefore, to increase substrate adhesion, we applied 60 s oxygen plasma to activate oxygen-containing groups on the surface membrane. The plasma-activated membranes were studied by X-ray photoelectron spectroscopy (XPS) to confirm the presence of oxygen-containing groups on the surface. Though cellulose substrate itself contains hydroxyl groups and surface carboxylic groups, plasma treatment on the nylon-6 coated membrane increases the hydroxyl (OH) and carboxylic (COOH) groups that improve the hydrophilic properties, resulting in better sample absorption. XPS survey spectra are presented in the SI section (Fig. S3) to compare the carbon (C) and oxygen (O) ratios before and after plasma treatment. The intensity of the oxygen (O 1s) peak increased, and the carbon (C 1s) peak (Fig. S3) decreased after the oxygen plasma exposure, suggesting the presence of more oxygen species in the nylon-6 polymer chain (hydrocarbon).[66] The oxygen content (atomic percentage) increased 35.29% after oxygen plasma on the surface of the membrane, whereas carbon content reduced 12.1% indicating the formation of oxygen-containing functional groups such as –OH, –COOH, and C=O *etc.* These newly formed C–OH, C–COOH, C–C=O groups improved the hydrophilic properties of the nylon-6 polymer-coated cellulose fabric membrane to facilitate the absorption biofluids. Fig. 4(A and B) shows the deconvolution of carbon (C 1s) core level spectra to be characterized further, specifying the different oxygen-containing functional groups on the membrane surface before and after plasma treatment activation. The XPS core-level carbon (C 1s) spectra of untreated nylon-6 membrane (Fig. 4A, left) indicate higher peak (C–C) intensity at 284.8 eV binding energy compared to the oxygen-containing carbon–oxygen peaks C–OH (286.49 eV), C=O (287.65 eV), and C–COOH (288.86 eV). On the other hand, the plasma-treated membrane (Fig. 4B, right) showed lower intensity in the C 1s peak (C–C) than oxygen-containing C–OH peak, confirming newly generated hydroxyl group on the surface along with carboxylic, and carbonyl groups upon plasma functionalization. Increasing polar functionalities on the membrane surface using the plasma-generated oxygen radicals improves the hydrophilic properties as well as increases the chemical interaction with the targeted metabolites from biofluids.

The hydrophilicity of the SPSE membrane was evaluated by water contact angle measurement, as presented in Fig. 4C. Hydrophilic materials show water contact less than 90° while hydrophobic materials show greater than 90°. The other factors that can change the water contact angle of a material are surface roughness, heterogeneity, and humidity, *etc.* The water contact angle of uncoated cellulose fabric substrate, 0.5% nylon-6 coated membrane without plasma treatment, and 0.5% nylon-6 coated membrane after 60 s oxygen plasma functionalization are 119.1°, 111.3°, and 59.5°, are shown in Fig. 4C. The plasma-treated membrane exhibited hydrophilic properties, as

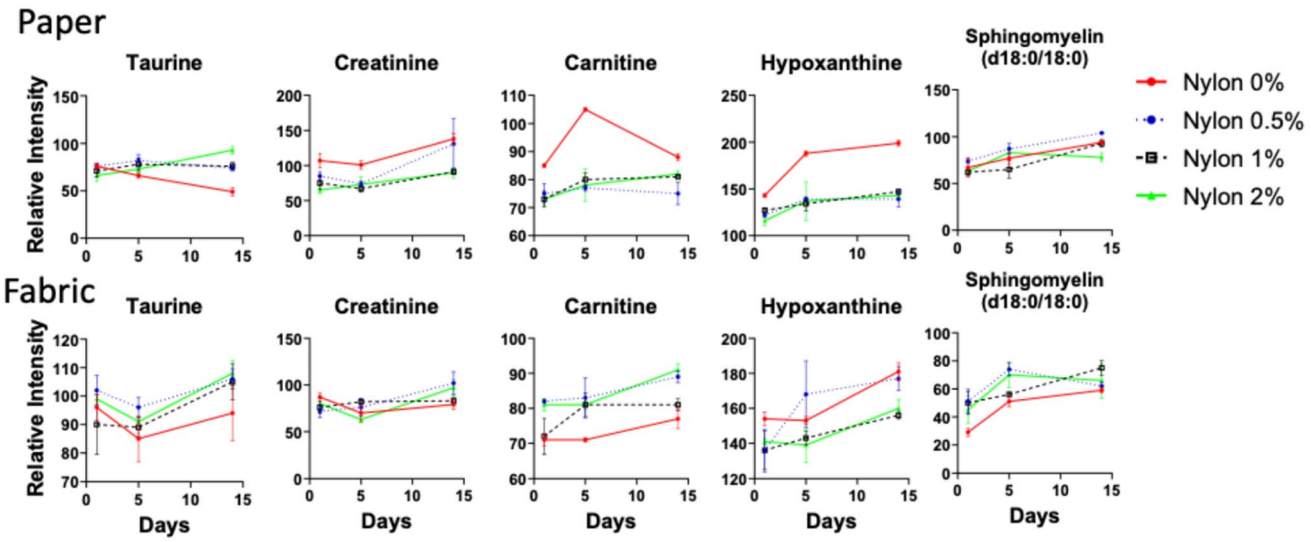

Fig. 5 Metabolite stability on paper (top) or fabric (bottom) membranes over the course of 1, 5, and 14 days. Values are expressed as percentage of signal compared to pure standards. ($n = 3$ per group, error bars represent standard deviation). *In vivo* irradiation.

indicated by a water contact angle of ≤90°, compared to both the bare cellulose substrate and the untreated nylon-6 coated membrane. We also tested the membrane by studying the absorption capacity of biological samples (whole blood and serum), as presented in Fig. 4D. All plasma-treated nylon-6 coated fabric membranes showed excellent absorption capacity for blood and serum compared to the uncoated cellulose substrate. Similar sample studies were performed for cellulose paper membranes, which are presented in the SI section (Fig. S4). All the paper membranes (coated and uncoated) showed outstanding absorption properties for all the biofluids such as blood, urine, and serum samples (Fig. S4). Uncoated cellulose paper substrate showed better sample absorptivity compared to cellulose fabric, which might be because of the different arrangement of cellulose microfibrils in the substrate. In cellulose paper substrates, fibers are thin and loosely oriented, whereas in the fabric or cloth substrates, cellulose fibers are tight and thick. Both fabric and paper membranes (plasma-treated) absorbed whole blood, serum, and urine samples within 30 seconds of its exposure.

Metabolite recovery and stability

We first tested metabolite recovery on SPSE membranes with both paper and fabric supports that were coated with three different substrates, including nylon-6, MC, and CA. The MC and CA sorbents had <55% recovery following a 1 day incubation period at room temperature for common polar metabolites typically identified in biofluids post-irradiation (Table S1). Thus, we restricted further testing to membranes with 0, 0.5, 1, and 2% nylon-6 sorbents and excluded MC and CA sorbents from additional analysis. The nylon-6 sorbents (0 and 0.5%) were also optimized for extraction solvent (50% ACN, 50% methanol, 40% ACN/40% methanol) and extraction time (5, 10, and 30 min). Both 50% ACN and 50% methanol gave a >60% extraction efficiency for polar metabolites, while 40% ACN/40% methanol gave >10-fold increase in signal from lipids extracted from the membranes (Table 2). A 5–10 min was sufficient for metabolite elution.

Metabolite stability was tested using spiked standards on paper and fabric cellulose membranes with 0, 0.5, 1, and 2% nylon-6 coatings as a measure of the percent recovery at 1, 5,

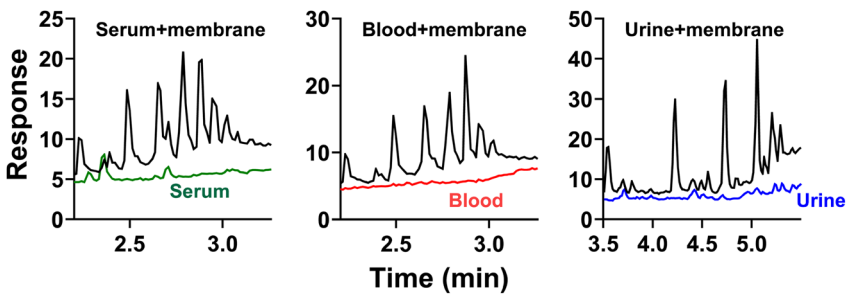

Fig. 6 Typical total ion chromatograms in positive ionization mode showing increased baseline noise are present in membrane samples for the serum, whole blood, and urine preparations. The chromatogram in black shows increased baseline noise from the membrane material. The chromatogram in green (serum), red (blood), or blue (urine) shows the typical baseline for these biofluids.

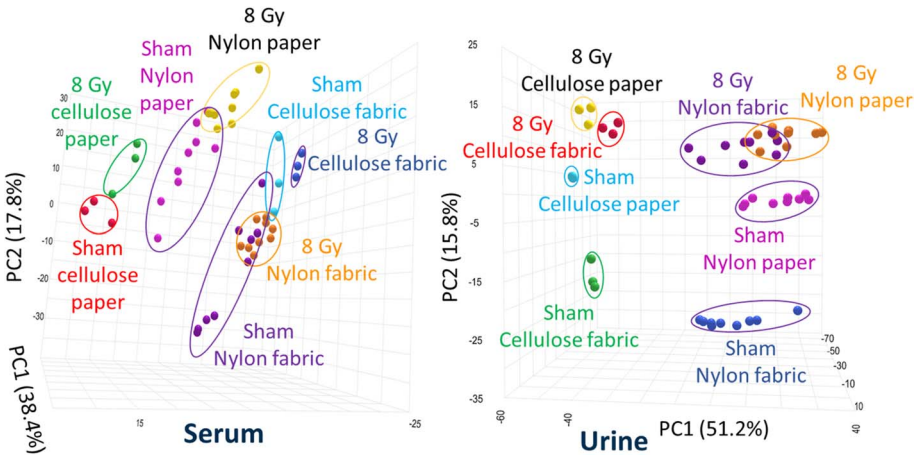

Fig. 7 PCA plots of serum (left) and urine (right) untargeted profiling shows successful separation of the radiation signature in biofluids from irradiated animals without matrix interference from the SPSE membranes.

and 14 days at room temperature compared to a freshly prepared standard solution (Fig. 5). Consistent with our previous recovery measurements, we found >50% metabolite recovery for the nylon-6 membranes. As they maintained consistent stability over a 14-days period at room temperature this demonstrates that SPSE membranes can preserve small molecule radiation biofluid signatures and be useful in a radiological emergency scenario. Interestingly, higher recovery was observed for hypoxanthine compared to the freshly prepared standard solution that indicates removal of some potential matrix effects. Overall, similar performance is maintained irrespectively of paper or fabric substrates or percentage of nylon-6 coating application, further testing was restricted to 0.5% nylon-6 coated paper membrane since it showed high

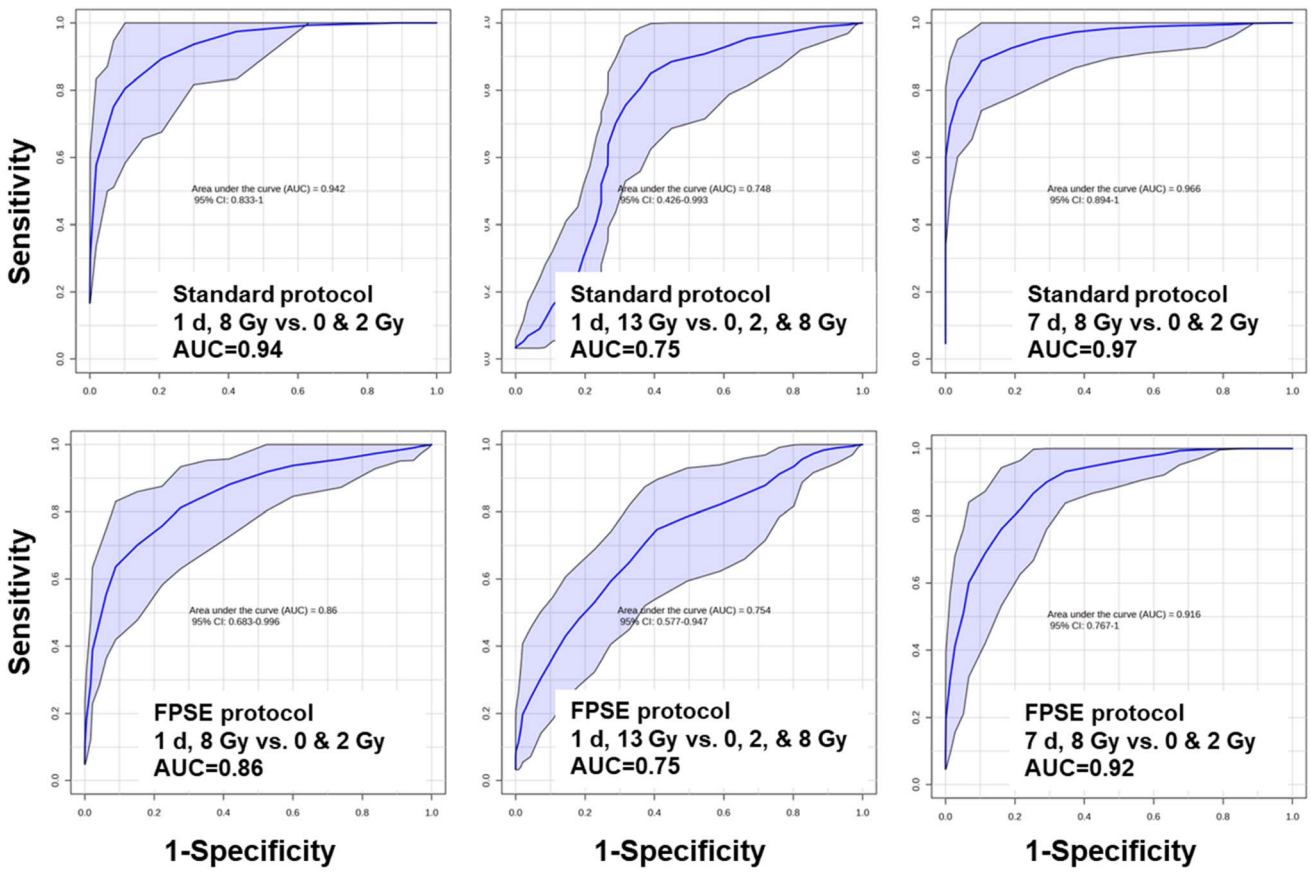

Fig. 8 Area under the receiver operating characteristic (AUC) curves show comparable sensitivity and specificity in mice exposed to IR irrespective of sample preparation protocols. (AUROC classification: excellent ≥0.9, very good ≥0.8, good ≥0.7).

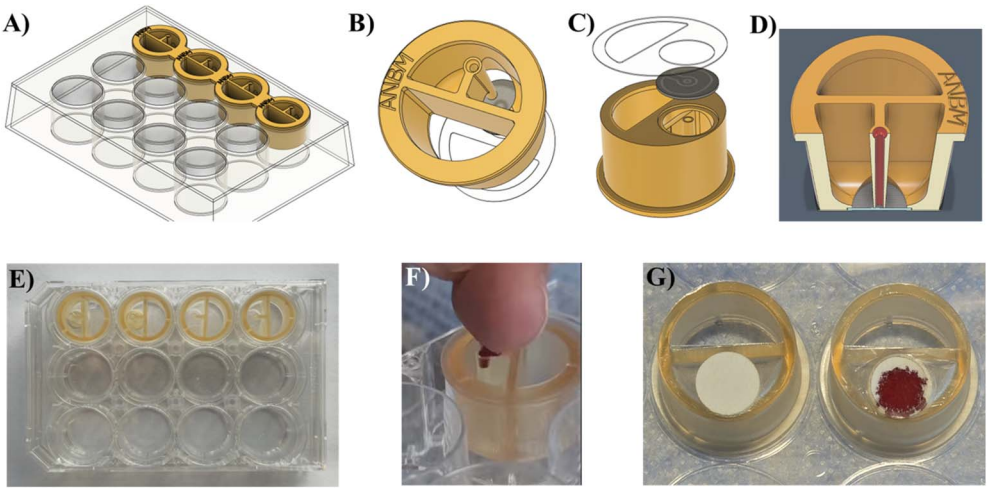

Fig. 9 A high throughput sample collection device for stabilizing and recovering radiation biomarkers. (A) A 12-well plate with 4-row-connected transwell strip configuration of blood collectors. (B) Front view of the individual transwell configuration, (C) assembly layer stack consisting of 3D printed transwell (bottom), membrane (middle), adhesive (top). (D) section-view of the heparin-treated blood capillary directing to the membrane, (E) an image of 12 well-plate sample collector with 4× of the individual transwell configuration. (F) A finger is pricked with a lancet, and a blood-drop is extended to the apical surface of the capillary to allow blood to be drawn in by capillary force and delivered to the membrane down-stream of the capillary. (G) Membranes before and after blood absorption through the microcapillary.

surface porosity and better sorptive properties compared to fabric membrane.

Untargeted metabolomics revealed minimal baseline noise is introduced when incorporating paper or fabric cellulose and nylon-6 membranes into standardized metabolomics sample preparation. Increased signal was observed in both ESI^+ and ESI^- between 2.2–3.5 min in whole blood and serum and 3.5–6.5 min in urine (Fig. 6), primarily for membranes with the nylon-6 sorbent (Fig. S5 and 6 shows chromatograms for the 13 min run for a whole blood sample). To determine how these minor artifacts could skew the spatial groups, we evaluated the untargeted sham and 8 Gy irradiated data sets using a PCA visualization tool. For serum, the first two vectors from a PCA plot accounted for 56.2% of the variation, while the first two vectors for urine accounted for 67.0% of the variation. Looking at the sham-irradiated samples in the PCA plot (Fig. 7), we observed that the membrane materials do shift the spatial distribution due to the presence of these artifacts. However, greater shifts in the radiation signature provide excellent separation at 1 day after 8 Gy IR exposure in the murine model.

Lastly, we utilized a targeted metabolomic assay to measure changes in biofluid metabolite concentrations and used ROC curve analysis to measure the area under the curve (AUC) and compare sensitivity and specificity between sample preparation methods. Urine, whole blood, and serum were collected from mice irradiated at 0, 2, 8, and 13 Gy at day 1 and 7 (0, 2, and 8 Gy). Nearly identical metabolite recovery and IR responses were observed in urine samples compared to urine applied to membranes (Fig. S7). For whole blood and serum, similar trends were observed for polar metabolites; however, wider variation was observed in sphingomyelin (SM) levels after membrane application indicating that extraction may vary among metabolite polarity. To test the sensitivity and specificity we combined a metabolite panel from eight metabolites found in urine (carnitine, TML, taurine, hypoxanthine) and blood (carnitine, citrulline, taurine, SM). The 0 and 2 Gy cohorts were combined as these groups both represent individuals needing minimal medical attention due to radiation injury when compared to an 8 or 13 Gy dose, which would represent an equivalent dose in humans to elicit hematopoietic or gastrointestinal syndrome. There was slightly lower performance for the membrane preparation protocol (AUC = 0.86) compared to the standard protocol (AUC = 0.94) when comparing the 8 Gy cohort to the combined 0 and 2 Gy cohorts at 1 day (Fig. 8). However, we found similar performance for both protocols when comparing the 13 Gy cohort to the combined 0, 2, and 8 Gy cohorts at 1 day (AUC = 0.75) and the 8 Gy cohort to the combined 0 and 2 Gy cohorts at 7 days (AUC = 0.97 and 0.94) (Fig. 8). With serum and urine biomarkers combined, slightly lower performance (AUC < 0.80) was observed for the 13 Gy cohort compared to the combined 0, 2, and 8 Gy cohorts at 1 day, but good to excellent results (AUC > 0.80) were achieved for the other groups and were comparable between our standard protocol and the membrane protocol (Fig. S8). It should be noted that there were sex specific differences in ROC performance, primarily with lower AUC values observed for the male 7 days 8 Gy *vs.* 0 and 2 Gy group and the female 1 day 8 Gy *vs.* 0 and 2 Gy group (Fig. S9).

A high-throughput point of care blood collection device was developed, assembling the SPSE membrane in a 12-well plate configuration (Fig. 9A). This point of care device can be used to collect samples (*e.g.*, whole blood) using finger stick and stabilize biomarkers at room temperature for up to two weeks. A multi-configuration, material-type customizable transwell insert was designed with a microcapillary (Fig. 9B) at the center to transport a blood drop from a finger to the SPSE membrane

that is assembled downstream (Fig. 9C). An orthographic section-rendering of the microcapillary in the transwell is presented in red that showcases the travel path and configuration (Fig. 9D). The design of the transwell strip was developed to self-collect the biofluid sample into the SPSE membrane while facilitating biomarker extraction directly in the same well plate device with solvent wash performed by automated instrumentation available in a standard clinical laboratory. All configurations of the insert have been designed for fabrication using injection molding for mass production or in the case of this study Stereolithography (SLA) resin printed using an autoclavable biocompatible Surgical Guide Resin (Form3B+, 100 μm layer thickness; FormLabs, MA, USA) and the capillary was chemically modified using UV-enhanced physisorption of heparin to make the surface more hydrophilic and prevent coagulation of the samples. Additionally, at the apical head of the capillary, the surface was modified using silane chemistry to form a hydrophobic inert coating, facilitating easy uptake of the sample into the microcapillary. Sorptive phase extraction membranes have been used previously as a biofluid sampler (dried blood spot card) to collect and prepare whole blood samples.[67]

The transwell has a secondary opening that can be used to collect the eluted biomarker solution for mass spectroscopy analysis. An image of 12 well plate sample collection device with 4× of the individual transwell is presented in Fig. 9E. The transwell can be used to collect any biofluid samples (whole blood, serum, urine) through the microcapillary into the SPSE membrane for metabolomic analysis. A blood-drop was collected using a lancet from a finger and extended to the capillary opening to allow blood to be drawn by the capillary force and absorbed into the membrane (Fig. 9F). The developed transwell insert showed excellent performance to deliver the blood sample into the membrane and an image of membranes before and after blood absorption is presented in Fig. 9G, indicating the collection of blood through the microcapillary. Our goal is to upgrade this device up to 96 well plate which can even faster the sample collection process after a radiological event.

Conclusions

Nylon-6 coated SPSE membranes feature a heterogenous surface porosity that leads to excellent absorption capacity and increased broad spectrum of metabolite recovery compared to our previous membrane designs and fabrication. These substrates increase metabolite stability at room temperature up to 2 weeks and could reduce the need for specialized refrigeration equipment in emergency scenarios. Additionally, sample storage will be important in the early stages of triage as specialized laboratories will be needed for sample processing. Signal suppression from membrane material does not interfere with separation of irradiated individuals when using the murine model. The sensitivity and specificity obtained from the AUC value from a ROC curve based on blood, serum, and urine was maintained with 0.5% nylon-6 coated membrane that was equivalent to a fresh biofluid preparation. Overall, this may prove to be useful technology in emergency situations and not limited to nuclear and/or radiological events, as cold chain management can complicate response logistics and transport to processing facilities may be delayed. The SPSE membrane has demonstrated promising performance for biomarker extraction and stabilization during initial testing in controlled laboratory conditions. While these results provide a strong foundation using murine biofluids, the next phase involves transitioning the technology to human biofluids and validating its efficacy across diverse clinical conditions in real-world settings. To enhance the project's utility for point-of-care applications, upcoming work will optimize the SPSE workflow for integration into high-throughput and automated platforms, including scaling the system to 96-well formats. Future studies will focus on developing membranes selective for specific biomarkers and improving sensitivity, prioritizing validation in human clinical samples under physiological conditions to support practical implementation of real-world biodosimetry.

Conflicts of interest

There are no conflicts to declare.

Data availability

The data that support the findings of this research are available from the corresponding author upon reasonable request. Data is also publicly available *via* the open-access NIAID repository ImmPort (the Immunology Database and Analysis Portal) under study_2024 accession SDY3644.

Supplementary information (SI): FT-IR spectra; SEM images; XPS spectra; biofluid absorption; biomarker recovery; ESI chromatogram; and ROC curves, *etc.* See DOI: https://doi.org/10.1039/d6ra00832a.

Acknowledgements

This work was supported by the National Institutes of Health (National Institute of Allergy and Infectious Diseases) grant U01AI148307 (P. I.'s Evagelia C. Laiakis and Frederic Zenhausern). The authors acknowledge the Lombardi Comprehensive Cancer Metabolomics Shared Resource (MSR), which are in part supported by Award Number P30CA051008 (P. I. Louis Weiner) from the National Cancer Institute. The authors would like to thank the Lombardi Comprehensive Cancer Metabolomics Shared Resource (MSR) for data acquisition. The content is solely the responsibility of the authors and does not necessarily represent the official views of the National Cancer Institute or the National Institutes of Health. The authors also acknowledge support from the engineering staff at the Center for Applied NanoBioscience & Medicine.

References

1 M. M. Satyamitra, D. R. Cassatt, B. A. Hollingsworth, P. W. Price, C. I. Rios, L. P. Taliaferro, T. A. Winters and A. L. DiCarlo, *Metabolites*, 2020, **10**, 1–28.

2 F. S. Ou, S. Michiels, Y. Shyr, A. A. Adjei and A. L. Oberg, *J. Thorac. Oncol.*, 2021, **16**, 537–545.
3 H. Zhao, C. Xi, M. Tian, X. Lu, T. J. Cai, S. Li, X. L. Tian, L. Gao, H. X. Liu, K. H. Liu and Q. J. Liu, *Dose Response*, 2020, **18**, 1–11.
4 N. Fontanals, F. Borrull and R. M. Marcé, *Adv. Sample Prep.*, 2023, **5**, 100050.
5 A. Taraboletti, M. Goudarzi, A. Kabir, B. H. Moon, E. C. Laiakis, J. Lacombe, P. Ake, S. Shoishiro, D. Brenner, A. J. Fornace and F. Zenhausern, *J. Proteome Res.*, 2019, **18**, 3020–3031.
6 E. L. Pannkuk, A. J. Fornace and E. C. Laiakis, *Int. J. Radiat. Biol.*, 2017, **93**, 1151–1176.
7 S. Qiu, Y. Cai, H. Yao, C. Lin, Y. Xie, S. Tang and A. Zhang, *Signal Transduct. Targeted Ther.*, 2023, **8**, 132.
8 E. C. Laiakis, in *Methods in Molecular Biology*, Humana Press Inc., 2019, vol. 1978, pp. 391–402.
9 E. C. Laiakis, K. Strassburg, R. Bogumil, S. Lai, R. J. Vreeken, T. Hankemeier, J. Langridge, R. S. Plumb, A. J. Fornace and G. Astarita, *J. Proteome Res.*, 2014, **13**, 4143–4154.
10 A. Giovanetti, R. Marconi, N. Awad, H. Abuzied, N. Agamy, M. Barakat, C. Bartoleschi, G. Bossi, M. Canfora, A. A. Elsaid, L. Ioannilli, H. M. Ismail, Y. A. Issa, F. Novelli, M. C. Pardini, C. Pioli, P. Pinnarò, G. Sanguineti, M. M. Tahoun, R. Turchi and L. Strigari, *Sci. Rep.*, 2021, **11**, 8118.
11 A. Gkikoudi, S. A. Kalospyros, S. Triantopoulou, S. Logotheti, V. Softa, C. Kappas, K. Theodorou, E. C. Laiakis, G. Manda, G. I. Terzoudi and A. G. Georgakilas, *Appl. Sci.*, 2023, **13**, 12564.
12 L. Nemzow, T. Boehringer, B. Bacon and H. C. Turner, *PLoS One*, 2023, 1–15.
13 E. L. Pannkuk, E. C. Laiakis, T. D. Mak, G. Astarita, S. Authier, K. Wong and A. J. Fornace, *Metabolomics*, 2016, **12**, 18.
14 A. K. Cheema, Y. Li, J. Moulton, M. Girgis, S. Y. Wise, A. Carpenter, O. O. Fatanmi and V. K. Singh, *Int. J. Radiat. Oncol. Biol. Phys.*, 2022, **114**, 310–320.
15 B. Tsogbadrakh, J. A. Jung, M. Lee, J. A. Lee and J. H. Seo, *Biochem. Biophys. Res. Commun.*, 2022, **599**, 51–56.
16 R. Tyagi, K. Maan, S. Khushu and P. Rana, *Sci. Rep.*, 2020, **10**, 16063.
17 E. C. Laiakis, D. Trani, B. H. Moon, S. J. Strawn and A. J. Fornace, *Radiat. Res.*, 2015, **183**, 382–390.
18 X. Wu, T. Zhu, H. Li, X. He and S. jun Fan, *Radiat. Med. Prot.*, 2021, **2**, 89–94.
19 P. Ostheim, A. Tichý, C. Badie, M. Davidkova, G. Kultova, M. M. Stastna, I. Sirak, S. Stewart, D. Schwanke, M. Kasper, S. A. Ghandhi, S. A. Amundson, W. Bäumler, C. Stroszczynski, M. Port and M. Abend, *Radiat. Res.*, 2024, **201**, 523–534.
20 E. C. Laiakis, S. J. Strawn, D. J. Brenner and A. J. Fornace, *Radiat. Res.*, 2016, **186**, 92–97.
21 E. C. Laiakis, D. Nishita, K. Bujold, M. M. Jayatilake, J. Bakke, J. Gahagen, S. Authier, P. Chang and A. J. Fornace, *Int. J. Radiat. Oncol. Biol. Phys.*, 2019, **105**, 843–851.
22 A. Tartaglia, T. Romasco, C. D'Ovidio, E. Rosato, H. I. Ulusoy, K. G. Furton, A. Kabir and M. Locatelli, *J. Pharm. Biomed. Anal.*, 2022, **209**, 114486.
23 M. Locatelli, N. Tinari, A. Grassadonia, A. Tartaglia, D. Macerola, S. Piccolantonio, E. Sperandio, C. D'Ovidio, S. Carradori, H. I. Ulusoy, K. G. Furton and A. Kabir, *J. Chromatogr., B: Anal. Technol. Biomed. Life Sci.*, 2018, **1095**, 204–213.
24 A. S. Balajee, C. Badie, A. Barry Flood, E. C. Laiakis, M. Marrale, N. Maltar-Strmečki, M. Port, S. G. Swarts, H. M. Swartz, F. Trompier, M. Valente, R. C. Wilkins and I. Yamaguchi, *Int. J. Radiat. Biol.*, 2025, 1–20.
25 R. G. Ingle, S. Zeng, H. Jiang and W. J. Fang, *J. Pharm. Anal.*, 2022, **12**, 517–529.
26 M. Locatelli, A. Kabir, M. Perrucci, H. Ibrahim Ulusoy, S. Ulusoy, N. Manousi, V. Samanidou, I. Ali, S. Irem Kaya, F. R. Mansour, A. Cetinkaya and S. A. Ozkan, *Microchem. J.*, 2024, **207**, 111903.
27 A. A. Aly and T. Górecki, *Molecules*, 2020, **25**, 1719.
28 M. Locatelli, A. Kabir, M. Perrucci, S. Ulusoy, H. I. Ulusoy and I. Ali, *Adv. Sample Prep.*, 2023, **6**, 100068.
29 F. R. Mansour, A. Bedair, F. Belal, G. Magdy and M. Locatelli, *Sustain. Chem. Pharm.*, 2025, 102051.
30 F. R. Mansour, J. Płotka-Wasylka and M. Locatelli, *Analytica*, 2024, **5**, 451–457.
31 F. R. Mansour, M. Locatelli and A. Bedair, *Sustain. Chem. Pharm.*, 2026, **49**, 102294.
32 F. R. Mansour, A. Bedair and M. Locatelli, *Adv. Sample Prep.*, 2025, 100164.
33 M. M. Satyamitra, D. R. Cassatt, B. A. Hollingsworth, P. W. Price, C. I. Rios, L. P. Taliaferro, T. A. Winters and A. L. Dicarlo, *Metabolites*, 2020, **10**, 1–28.
34 D. L Chan, D. Fritz, M. McMahon, W. Peterson and T. Nessler, *J. Mil. Veterans' Health.*, 2023, **31**, 7–12.
35 Á. I. López-Lorente, F. Pena-Pereira, S. Pedersen-Bjergaard, V. G. Zuin, S. A. Ozkan and E. Psillakis, *Trends Anal. Chem.*, 2022, **148**, 116530.
36 T. Liu, J. Hu, A. C. Hasnain, P. Akarapipad, A. Varon, D. J. M. Park, H. Lei, K. Hsieh and T.-H. Wang, *Biosens. Bioelectron.*, 2025, 118071.
37 A. Kabir, R. Mesa, J. Jurmain and K. G. Furton, *Separations*, 2017, **4**, 21.
38 A. Ferracane, N. Manousi, A. Kabir, K. G. Furton, A. Mondello, P. Q. Tranchida, G. A. Zachariadis, V. F. Samanidou, L. Mondello and E. Rosenberg, *Sci. Total Environ.*, 2024, **906**, 167353.
39 B. Olayanju, A. Kabir and K. G. Furton, *Microchem. J.*, 2024, **196**, 109619.
40 N. Fontanals, F. Borrull and R. M. Marcé, *Adv. Sample Prep.*, 2023, **5**, 100050.
41 Y. Ekin Dolaksız, M. S. Kaynak, A. Kabir, K. G. Furton and M. Çelebier, *ACS Omega*, 2024, **9**, 18995–19002.
42 P. Prajapati, N. Patel and D. Kankva, *J. Pharm. Biol. Sci.*, 2024, **11**, 117–124.
43 A. Tartaglia, S. Covone, E. Rosato, M. Bonelli, F. Savini, K. G. Furton, I. Gazioglu, C. D'Ovidio, A. Kabir and M. Locatelli, *Adv. Sample Prep.*, 2022, **3**, 100022.

44 A. Taraboletti, M. Goudarzi, A. Kabir, B. H. Moon, E. C. Laiakis, J. Lacombe, P. Ake, S. Shoishiro, D. Brenner, A. J. Fornace and F. Zenhausern, *J. Proteome Res.*, 2019, **18**, 3020–3031.
45 E. C. Tanasescu, A. G. Ene, E. Perdum, O. Iordache and L. O. Secareanu, *Heliyon*, 2024, **10**, 1020.
46 A. Castiñeira-Landeira, L. Vazquez, A. M. Carro, M. Celeiro, A. Kabir, K. G. Furton, T. Dagnac and M. Llompart, *Microchem. J.*, 2024, **196**, 109542.
47 N. Manousi, A. Ferracane, N. P. Kalogiouri, A. Kabir, K. G. Furton, P. Q. Tranchida, G. A. Zachariadis, L. Mondello, V. F. Samanidou and E. Rosenberg, *Food Chem.*, 2023, **424**, 136423.
48 W. Chen, Y. Mei, S. Peng and X. Li, *Food Anal. Methods*, 2022, **15**, 1011–1025.
49 M. Locatelli, A. Tartaglia, H. I. Ulusoy, S. Ulusoy, F. Savini, S. Rossi, F. Santavenere, G. M. Merone, E. Bassotti, C. D'Ovidio, E. Rosato, K. G. Furton and A. Kabir, *Anal. Chem.*, 2021, **93**, 1957–1961.
50 X. Ruan, L. Xing, J. Peng, S. Li, Y. Song and Q. Sun, *RSC Adv.*, 2020, **10**, 10854–10866.
51 H. I. Ulusoy, E. Şahin, Ü. Polat, S. Ulusoy, M. Locatelli and A. Kabir, *Microchem. J.*, 2024, **197**, 109807.
52 R. Jain, B. Jain, A. Ghosh, D. Basu, A. Kabir, N. Ali, A. F. AlAsmari and S. Sharma, *Microchem. J.*, 2024, **203**, 110851.
53 N. Manousi and G. A. Zachariadis, *Molecules*, 2020, **25**, 2182.
54 N. Manousi, A. Kabir, K. G. Furton, E. Rosenberg and G. A. Zachariadis, *RSC Adv.*, 2022, **12**, 7149–7156.
55 M. Pouyan, G. H. Rounaghi and B. Deiminiat, *Microchem. J.*, 2024, **198**, 110119.
56 G. Heena, S. Rani, A. K. Malik, A. Kabir and K. G. Furton, *J. Chromatogr.*, 2016, **7**, 1000327.
57 M. E. Rosa, M. S. M. Mendes, D. C. V. Belchior, J. A. P. Coutinho, F. A. e Silva and M. G. Freire, *Adv. Sample Prep.*, 2024, **10**, 100058.
58 R. Jain, B. Jain, A. Kabir, A. Bajaj, R. Ch and S. Sharma, *Adv. Sample Prep.*, 2023, **6**, 100058.
59 V. Kazantzi and A. Anthemidis, *Separation*, 2017, **4**, 20.
60 M. Perrucci, E. M. Ricci, M. Locatelli, I. Ali, F. R. Mansour, A. Kabir and H. I. Ulusoy, *Adv. Sample Prep.*, 2025, **14**, 100182.
61 M. Locatelli, S. Covone, E. Rosato, M. Bonelli, F. Savini, K. G. Furton, I. Gazioglu, C. D'Ovidio, A. Kabir and A. Tartaglia, *Forensic Chem.*, 2022, **31**, 100460.
62 V. K. Singh, T. M. Seed and A. K. Cheema, *Expert Rev. Mol. Diagn.*, 2021, **21**, 641–654.
63 O. M. Kolawole, W. M. Lau and V. V. Khutoryanskiy, *Int. J. Pharm.*, 2018, **550**, 123–129.
64 Z. Pang, J. Chong, G. Zhou, D. A. De Lima Morais, L. Chang, M. Barrette, C. Gauthier, P. É. Jacques, S. Li and J. Xia, *Nucleic Acids Res.*, 2021, **49**, 388–396.
65 Z. Pang, Y. Lu, G. Zhou, F. Hui, L. Xu, C. Viau, A. F. Spigelman, P. E. Macdonald, D. S. Wishart, S. Li and J. Xia, *Nucleic Acids Res.*, 2024, **52**, W398–W406.
66 R. Thompson, D. Austin, C. Wang, A. Neville and L. Lin, *Appl. Surf. Sci.*, 2021, **544**, 148929.
67 M. Locatelli, A. Tartaglia, F. D'Ambrosio, P. Ramundo, H. I. Ulusoy, K. G. Furton and A. Kabir, *J. Chromatogr. B*, 2020, **1143**, 122055.